Journal of Physics: Conference Series **528** (2014) 012040 doi:10.1088/1742-6596/528/1/012040

In-beam test of the Boron-10 Multi-Grid neutron detector at the IN6 time-of-flight spectrometer at the ILL

J. Birch[1], J.-C. Buffet [2], J.-F. Clergeau[2], J. Correa[2], P. van Esch[2], M. Ferraton[2], B. Guerard[2], J. Halbwachs[2], R. Hall-Wilton[3], L. Hultman[1], C. Höglund[1,3], A. Khaplanov[2,3], M. Koza[2], F. Piscitelli[2], M. Zbiri[2]

[1] Linköping University, Thin Film Physics Division, IFM, SE-581 83 Linköping, Sweden
[2] Institute Laue Langevin, Rue Jules Horowitz, FR-38000 Grenoble, France
[3] European Spallation Source ESS AB, P.O Box 176, SE-221 00 Lund, Sweden

E-mail: anton.khaplanov@esss.se

Abstract.

A neutron detector concept based on solid layers of boron carbide enriched in ^{10}B has been in development for the last few years as an alternative for ^{3}He by collaboration between the ILL, ESS and Linköping University. This Multi-Grid detector uses layers of aluminum substrates coated with $^{10}B_4C$ on both sides that are traversed by the incoming neutrons. Detection is achieved using a gas counter readout principle. By segmenting the substrate and using multiple anode wires, the detector is made inherently position sensitive. This development is aimed primarily at neutron scattering instruments with large detector areas, such as time-of-flight chopper spectrometers. The most recent prototype has been built to be interchangeable with the ^{3}He detectors of IN6 at ILL. The ^{10}B detector has an active area of $32 \times 48\,cm^2$. It was installed at the IN6 instrument and operated for several weeks, collecting data in parallel with the regularly scheduled experiments, thus providing the first side-by-side comparison with the conventional ^{3}He detectors. Results include an efficiency comparison, assessment of the in-detector scattering contribution, sensitivity to gamma-rays and the signal-to-noise ratio in time-of-flight spectra. The good expected performance has been confirmed with the exception of an unexpected background count rate. This has been identified as natural alpha activity in aluminum. New convertor substrates are under study to eliminate this source of background.

1. Introduction

The Multi-Grid is a novel detector for thermal neutrons. It is based on thin solid converter layers of $^{10}B_4C$. The detector concept has been developed at the ILL in collaboration with the ESS in order to meet the requirements of upcoming neutron scattering instruments where detector areas of many square meters will be required. Cold and/or thermal Time-of-Flight (ToF) spectrometers in particular require a sensitive area of the order of $30\,m^2$, and it is at these instruments that the Multi-Grid design is particularly targeted. As can be seen in the ESS Technical Design Report [1], 3 instruments of this type may be expected to be built at the ESS. While previously such detector arrays [2] have been built with ^{3}He as the converting

Figure 1. In this image of the detector, the B_4C layers are horizontal and neutrons arrive from the top.The 6 modules of 16 grids each form an assembly of 360 gas-filled tubes, 24 tubes wide and 15 deep, which are visible on the front side. Each tube is readout by an anode wire.

medium, this option is likely unfeasible in the future due to a very limited world-wide supply of ^{3}He [3, 4, 5, 6], therefore new technology is required.

1.1. Multi-Grid detector

Descriptions and characterization of the previous Multi-Grid prototypes have been published [7, 8, 9, 10]. Here, we report on the first test of this technology in the time-of-flight spectrometer IN6 at ILL.

The present detector is composed of 6 modules of 16 grids as shown in figure 1. Each grid is composed of 14 so-called *blades* which are coated on both sides with $1\,\mu m$ of $^{10}B_4C$ [12] and mounted orthogonally to the direction of the incoming neutrons. The other surfaces are not coated. The unit cell of a grid has a $20 \times 20\,mm^2$ sensitive area and $10\,mm$ depth. When a stack of 16 grids is assembled, 60 rectangular tubes are formed. These are readout by anode wires. Signals are readout from both the anode wire and the individual frames. Coincident signals are recorded and define 3-D positions of detected neutrons. The depth of the interaction is necessary since in ToF applications, the exact flight distance of each neutron must be known in order to reconstruct its velocity.

Grids were connected 3-by-3 together with their neighbours from the adjacent modules and readout by a single amplifier. The anode wires were connected using resistances in charge division chains. Each such chain contained 30 wires which run from the back of the detector to the front, connect to a neighbouring set of tubes and then run from the front of the detector to the back. In this arrangement, the discrete channel information corresponding to the detector depth was converted to analogue information and some ambiguity may arise as to the exact wire that has detected an event. Note, however, that no such ambiguity exists in the other 2 dimensions. In total, only 32 channels were required to readout all frames and 24 channels to readout all wires (2 ends of 12 charge division chains). With this setup, the new detector was readout with a similar number of channels as the present IN6 detectors.

In order to limit the effect of neutron scattering in the detector, the 6 modules were shielded

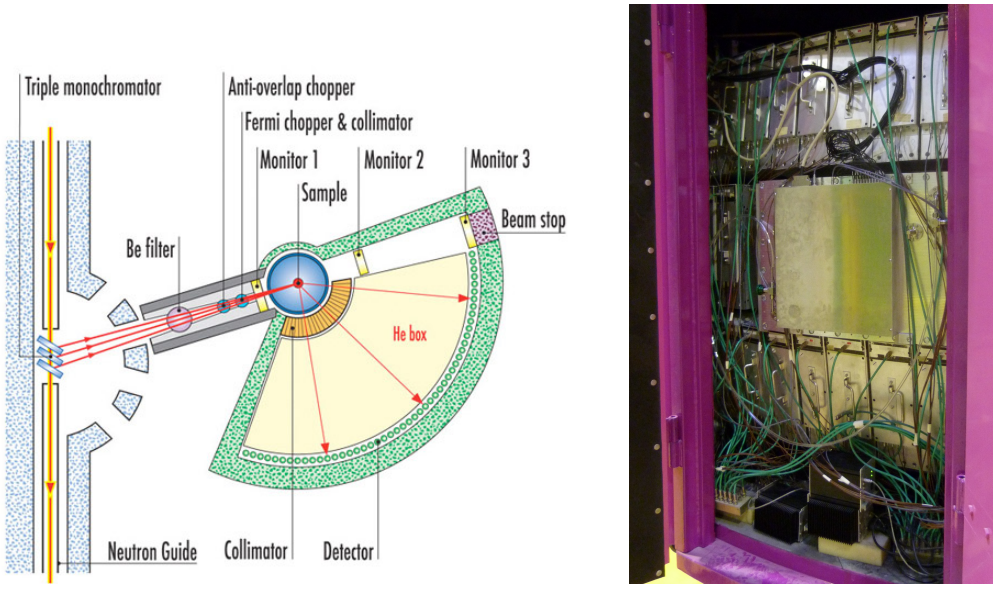

Figure 2. Left: The geometry of IN6. **Right:** The Multi-Grid detector installed at the instrument. ^{3}He modules can be seen above and below the ^{10}B detector.

from each other by sheets of cadmium. The sides of the detector were additionally shielded. The detector was filled with 1 *bar* of $ArCO_2$ 90/10 mixture. The gas was continually flushed during the operation.

1.2. IN6 instrument

IN6 is a cold neutron time-focusing time-of-flight chopper spectrometer at the ILL. Its layout is shown in figure 2. The incident neutron wavelength can be selected by adjusting the monochromator orientation to the Bragg condition for 4.1, 4.6, 5.1 and 5.9 $\AA$. A chopper system defines pulses incident on sample. The detector array has a sensitive area of $4\,m^2$ and detects neutrons in the scattered angular range of $10° - 115°$. The neutron flight path from the sample to the detectors is $248\,cm$. By measuring both the angular and temporal spread of the detected neutrons, both momentum and energy transfer between scattered neutrons and the sample can be determined. More information about the instrument is available at the ILL website [11].

The IN6 detector comprises 337 ^{3}He tubes arranged in 3 tiers and angled so that each tube is tangential to the cone of neutrons scattered at the same angle. The tubes are compressed so that their width is $32\,mm$ and the depth is $16\,mm$. The pressure of ^3He is $3\,bar$. The ^{10}B detector replaced a total of 25 ^{3}He tubes in the middle tier at scattering angles of approximately $95 - 105°$ as shown in figure 2. This configuration was operated for several weeks, including 2 weeks of beam time, during which regular experiments were performed using the wavelength setting of 5.1 $\AA$. Additionally, dedicated detector tests were carried out at wavelength 4.1 and 4.6 $\AA$.

2. Results of measurements at IN6

2.1. Efficiency

Efficiency of a neutron detector based on multiple layers of solid converters depends on the thickness of the layers. In order to obtain an optimal efficiency, two parameters – the probability of conversion and the probability to detect secondary particles – must be balanced. The

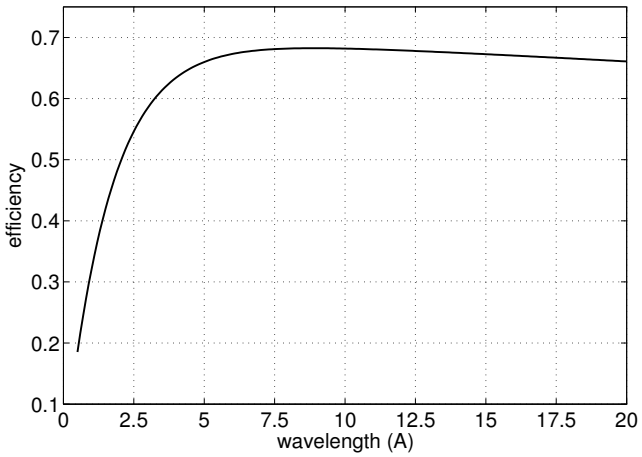

Figure 3. Calculated efficiency for the Multi-Grid detector with 28 $^{10}B_4C$ layers of $1\mu m$ as a function of neutron wavelength.

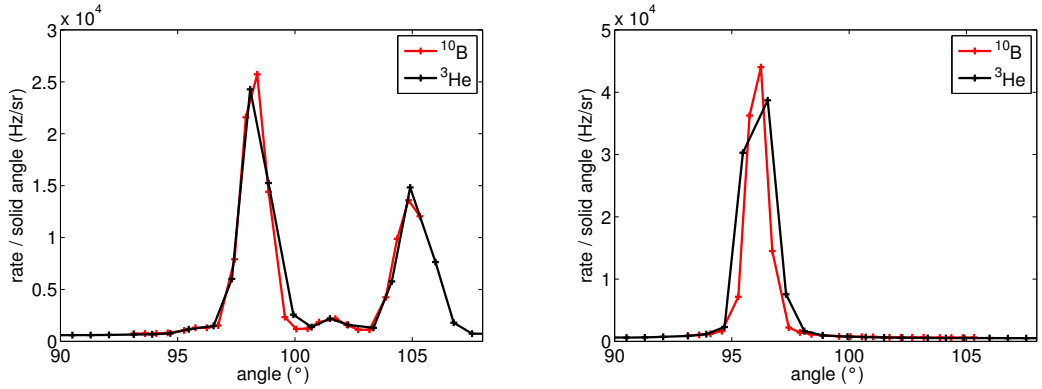

Figure 4. Angular distributions obtained with ^{3}He tubes and Multi-Grid detector. **Left:** 4.1 $\mathring{A}$ and **right:** 4.6 $\mathring{A}$ incident wavelength.

optimal value depends on the neutron wavelength. With $^{10}B_4C$ layers of $1\mu m$, the detector is optimized for 2.5 $\mathring{A}$. We therefore expect that the Multi-Grid should have an advantage at these lower wavelengths. Measurements with monochromatic neutrons of 2.5 $\mathring{A}$ at the CT1 and CT2 beam lines at the ILL have shown that the efficiency of modules used in the IN6 prototype is $\approx 50\%$ [7, 8, 9]. The efficiency can be calculated for a range of neutron wavelengths [13], this is shown in figure 3.

During the IN6 test, it was also possible to make a relative comparison to the efficiency of the ^{3}He detectors. Measurements were carried out at 4.1 $\mathring{A}$ and 4.6 $\mathring{A}$ incident wavelengths, using samples of yttrium garnet and silicon respectively. These combinations of wavelengths and samples resulted in Bragg scattering of neutrons into the Multi-Grid detector. In this way the wavelength of the majority of detected neutrons is known and the rate is significantly higher than for neutrons scattered inelastically.

Figure 4 shows the neutron rate as a function of scattering angle for the Multi-Grid prototype and the ^{3}He tubes in the same angular range. Here we consider the rate per solid angle. Each point in figure 4 shows the counts registered in a tube divided by the solid angle of that tube as

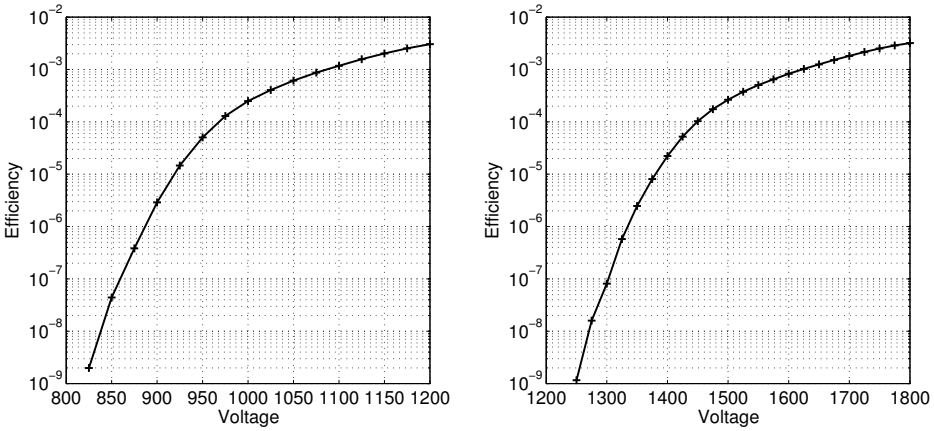

Figure 5. Measurement of the γ-ray efficiency with the Multi-Grid (left) and a ^{3}He detector (right) as a function of bias voltage. The nominal operating voltages for these detectors are $850\,V$ and $1350\,V$ respectively (as determined prior to this measurement).

a function of the angular position of the tube with respect to the sample.

Next we compare efficiencies including the effects of the dead spaces specific to each detector for a given wavelength. The counts are integrated over the range of tubes in which a Bragg peak is emitted. The ratio $rate(^{10}B)/rate(^3He)$ is 1.09 at $4.1\,\mathring{A}$, and 0.97 at $4.6\,\mathring{A}$. This means that the Multi-Grid detector is globally only 3% less efficient than the IN6 detection system at $4.6\,\mathring{A}$, and 9% more efficient at $4.1\,\mathring{A}$. This is in agreement with the optimization of the Multi-Grid for lower wavelengths.

2.2. Gamma-ray sensitivity

The sensitivity of neutron detectors to gamma-rays is an important characteristic since neutron scattering instruments are subject to a strong gamma flux originating from the instrument itself and from other sources such as the surrounding neutron guides and other instruments. γ-rays may interact in the detector, inducing unwanted signals and decreasing the signal-to-background ratio.

Gamma-ray discrimination in both the ^{10}B and ^{3}He detectors is based on the fact that the gamma photons are not likely to deposit more than a few tens of keV in the detector, whereas neutron interactions lead to larger energy deposits (up to $1.8\,MeV$ in the case of ^{10}B converter). This is because γ-rays are detected through secondary electrons while neutrons are detected through secondary ions interacting with the gas, therefore leading to a large difference in the energies deposited over a finite distance.

Gamma sensitivity measurements have been performed on a number of Multi-Grid prototypes [14]. Figure 5 shows the efficiency to detect a $662\,keV$ γ-ray measured with a $164\,MBq$ ^{137}Cs source, as the function of the high voltage, and, therefore, gas amplification gain, with a fixed value of the threshold. We see that at the typical bias voltage of $850\,V$ (for $1\,bar$ of $ArCO_2$), γ-ray efficiency is below 10^{-7} and can be improved by another order of magnitude if the voltage is lowered by $25\,V$. For comparison, figure 5 also shows the γ-ray efficiency for a ^{3}He detector measured with the same source (this is not an IN6 detector). While the γ-ray energy does influence the detection efficiency, the dependance is rather weak [14].

Taking advantage of the ToF information provided by the IN6 instrument allows validating the low γ-ray sensitivity in an alternative way. A large portion of the γ background inside the

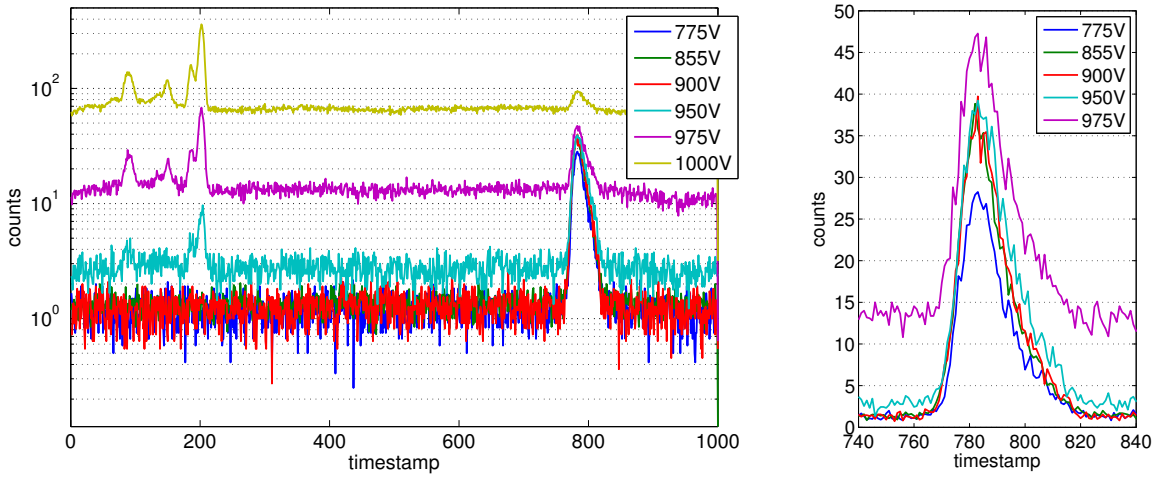

Figure 6. Time spectra measured for different values of the high voltage. **Left:** the full time scale corresponding to 6 ms. Peaks on the left were verified to correspond to γ-rays using a NaI detector. The peak on the right is due to the elastic neutrons. **Right:** the neutron peak in linear scale. Note the loss of neutron counts for the lowest voltage.

IN6 chamber comes from the components of the instrument itself, due to nuclear interactions of neutrons with the different elements of the instrument (choppers, sample, beam stop). This gamma background is therefore associated with a well defined time structure, as was observed in the measurement and can be seen on figure 6. The ToF spectrum in this figure was measured for several values of the high voltage. It is not corrected for the detector depth, since here we are interested in photons which travel at the speed of light. At each voltage, an elastic neutron peak is seen at about timestamp 800. The peaks at timestamp 200 and below can be seen only when the high voltage reaches $950\,V$. These are due to γ-rays. The time structure of these peaks implies that they are generated by the pulsed neutron beam of IN6 as it passes the absorbing components of the instrument. Of the constant γ rate, $\approx 2/3$ is due to the instrument, possibly emitted in the chopper closed state when the entire beam is absorbed.

The time spectrum in figure 6 was verified using a NaI scintillator detector placed adjacent to the ^{10}B prototype. The neutron peak cannot be seen in the photon detector, but the γ peaks are identical. This detector also allowed to estimate that on the order of 10^6 γ-rays impinge on the Multi-Grid prototype every second. No peaks corresponding to these γ-rays were found in any neutron time of flight spectra with high voltage of $900\,V$ and below.

2.3. Background

Photons are not the only source of background in a neutron detector. Indeed, in during the IN6 test, it became clear that a different background was present – one corresponding to significantly higher pulse heights than γ-rays. Figure 7 compares ToF spectra taken simultaneously with the ^{10}B and ^{3}He detectors. While the physical signal is evident in the Multi-Grid data and matches that measured by ^{3}He, the background level is higher. This background is not modulated when the beam is pulsed and is present irrespective of the instrument's shutter state or even the reactor operation. Subtracting a constant background, corresponding to $4.4\,Hz$ distributed over the whole detector, from the ^{10}B data, reproduces the ^{3}He data, although of course, with a higher statistical noise level.

The anode wire pulse height spectrum of the background is compared to the spectrum

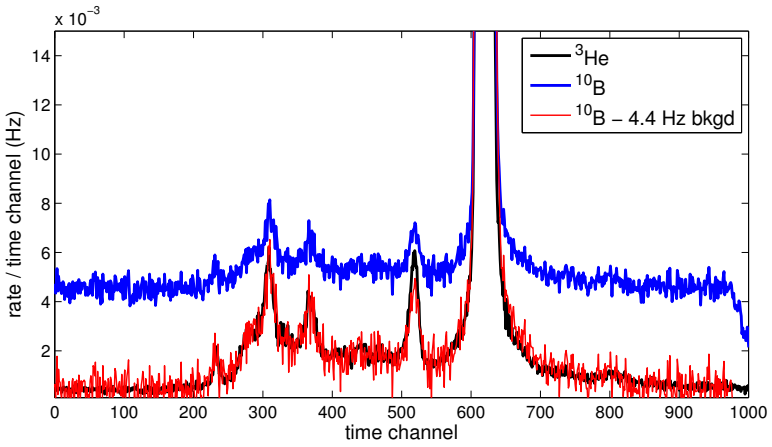

Figure 7. Time spectra obtained with ^{3}He detectors (black curve) and Multi-Grid detector (blue curve). The red curve is obtained by subtracting a flat 4.4 Hz background from Multi-Grid data in order to match the ^{3}He data.

corresponding to neutrons in figure 8. We see that energy of the majority of background events overlaps with the neutron events and some have higher energies. The background spectrum has a shape characteristic of a strong wall-effect (*i.e.* of particles stopped by the walls surrounding the gas volume before depositing the full energy in the gas). This is inconsistent with secondary atmospheric particles created by cosmic rays, since at Earth's surface, most of these are minimum ionizing and the expected energy deposit is similar to that of γ-rays – at most tens of keV for this size of the gas chamber. Furthermore, cosmic ray particles are more likely to be traveling vertically, and therefore would deposit more energy when a gas tube is also oriented vertically. The rate of the background, however, was constant for both vertical and horizontal orientations. We therefore exclude cosmic rays as the source of this background.

The background pulse height spectra do, however, closely resemble spectra of α particles. Figure 8 also shows simulated spectra of α particles emitted from the frames, where α are emitted from a random depth in the aluminium and in a random direction. The energies of the α's simulated correspond to those emitted by decay chains starting at 4 isotopes. The two most common primordial α-emitters, ^{232}Th and ^{238}U are shown as well as the relatively long-lived radium isotopes produced as a result of their decay. We see that the simulated spectra are qualitatively consistent with measurement, in particular the shape of the high-energy tail of the spectrum and its end-point at about $3\,MeV$. The likely source of such emissions are the naturally-occurring concentrations of uranium and thorium in aluminium. These undergo a chain of decays before arriving at a stable isotope, emitting 7-8 α in the process. The alpha energies vary between 4 and $9MeV$.

Contamination of aluminum by uranium and thorium isotopes and their decay daughters has been studied in the past [15, 16, 17]. Corresponding rates for standard aluminium alloys were found to be between 0.05 and $0.25\,cm^{-2}h^{-1}$, which for this configuration of Multi-Grid detector, leads to total rates over the whole detector between $0.96\,Hz$ and $4.8\,Hz$, consistent with what was measured experimentally.

This background level is presently the main concern in the framework of developing the Multi-Grid technology for large area position sensitive detectors for inelastic instruments. Two solutions are currently being investigated to eliminate this background. One is to deposit a thin nickel layer at the surface of aluminium in order stop the alpha particles before they reach the gas. Another solution is to use U/Th-free aluminium for which the concentration of uranium

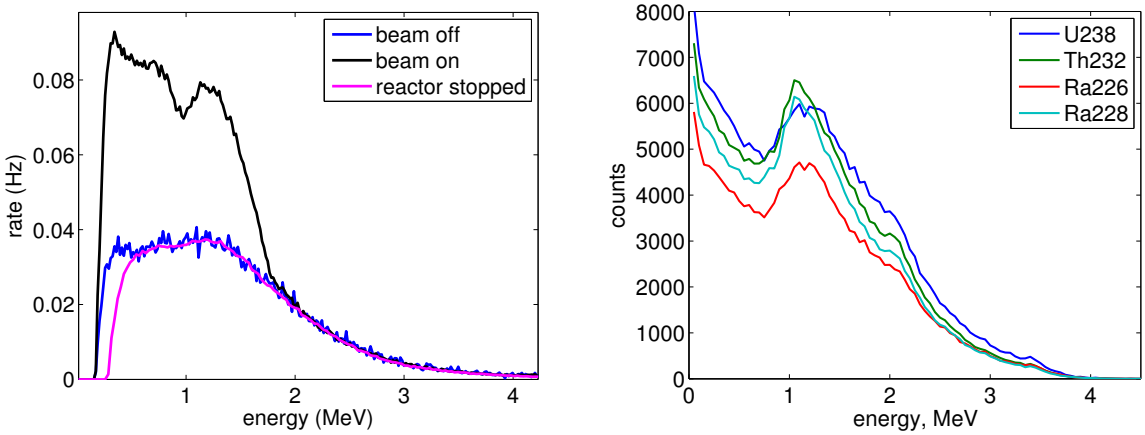

Figure 8. Left: energy spectra obtained in the Multi-Grid detector in IN6. With beam on, a characteristic spectrum of secondary particles emitted from the conversion layer is evident, however, it is superimposed with a higher-energy spectrum. With beam stopped, the spectrum no longer resembles that of neutrons. Note that a different threshold was used in the *beam on/off* and *reactor stopped* measurements. **Right:** Monte-Carlo simulation of energy spectra produced by α particles in the gas, emitted in the walls of the detector for different primary contaminants.

and thorium is 2-3 orders of magnitude lower than in standard aluminium alloys.

2.4. Neutron scattering in aluminium

The advantage of using aluminium for construction of the Multi-Grid detectors is its transparency for thermal neutrons. However, the scattering cross section in aluminium cannot be totally neglected, and may induce undesirable geometrical and temporal effects. Two measurements were carried out at 4.1 $\mathring{A}$ and 4.6 $\mathring{A}$ to observe these effects. For these wavelengths, Bragg reflection is allowed in aluminium. These measurement are compared to those at 5.1 $\mathring{A}$ in figure 9, where count rate is shown as a function of time and depth of the detector. The maximum of the elastic peak is moving toward larger time-of-flight values with increasing depth, due to an increased flight path inside the detector. The slope of the curve giving the position of the maximum of the elastic peak as a function of depth is directly correlated with the velocity of elastically scattered neutrons.

A secondary distribution of a much lower intensity moves toward higher ToF values with decreasing depth, which is characteristic of neutrons traveling with a negative velocity (from the back to the front of the detector). These neutrons are therefore identified as elastically scattered neutrons in the back of the frames. There is a large block of aluminium at the rear of the frame, which leads to this visible scattering effect. Figure 10 shows the time spectrum obtained for the whole detector after time correction. The broadening of the base of the elastic peak toward larger ToF values is a consequence of this effect. Note, that as expected, it is not present for neutron wavelength of 5.1 $\mathring{A}$. In the future versions of the Multi-Grid, cadmium shielding can be used directly behind the last boron layer in order to minimize this effect. Additionally, other aluminium parts of the frame will be thinner. Furthermore, absorbing material can be considered on the elements of the frames parallel to the neutron flux.

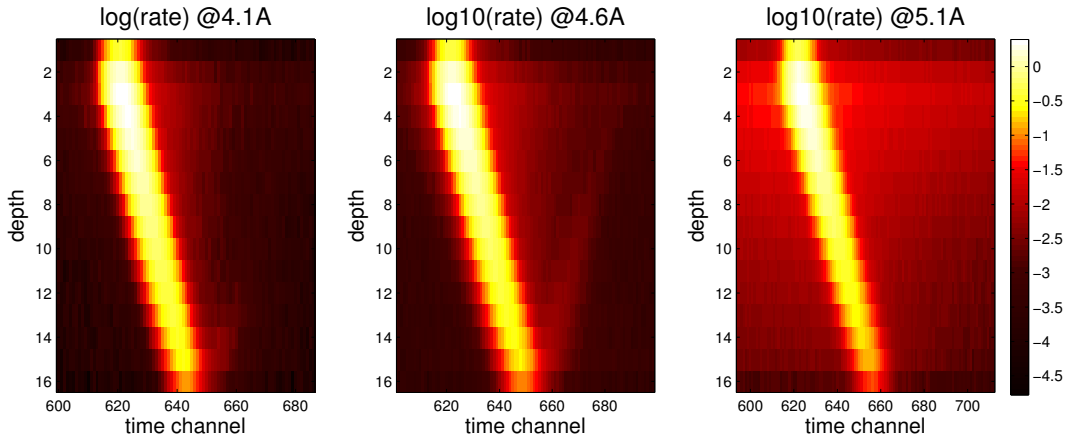

Figure 9. Time spectra measured as a function of depth (cell number) for 4.1 $\mathring{A}$, 4.6 and 5.1 $\mathring{A}$ incident neutron wavelengths.

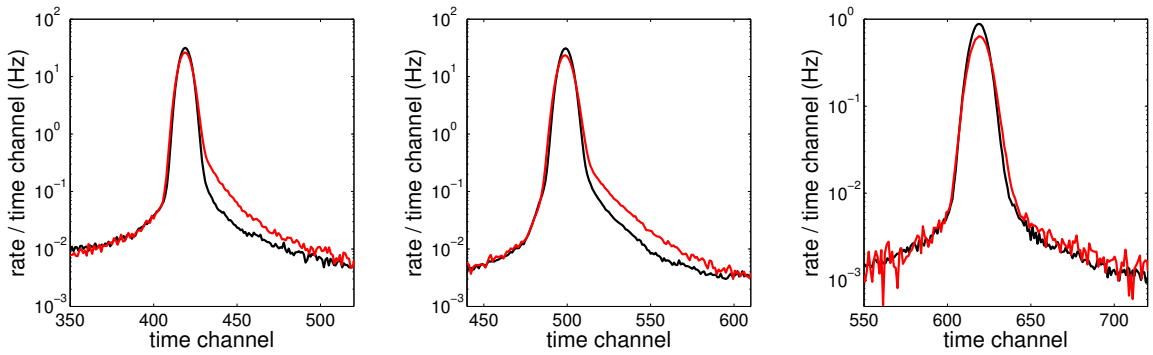

Figure 10. Time spectrum measured in the Multi-Grid detector (red) compared to the IN6 setup (black), from left to right – for 4.1, 4.6 and 5.1 $\mathring{A}$. The enlargement of the base of the elastic peak is a consequence of scattering in aluminum.

3. Conclusion and Outlook

In combination with previous characterization studies of Multi-Grid prototypes, the in-beam test at IN6 at the ILL provides encouraging results. We have demonstrated that the new detector is able to reproduce the measurements currently done with ^3He detectors. In particular, efficiency, time resolution and γ-ray sensitivity are all already competitive. The contribution of scattered neutrons has been identified as expected. There are clear possibilities for improvement here, although some amount of scattering must be accepted as it must in any detector.

Due to the multi-layer nature of the ^{10}B detector, there are two aspects in which the Multi-Grid differs from conventional ^{3}He detectors. Firstly, the ratio of the internal surfaces to the active area of the detector is about an order of magnitude greater than for a single tube. Therefore, also the impact of radioactive contamination of the materials is likewise enhanced. Aluminium, the material chosen due to favourably low cross sections and cost, naturally contains more α emitters than other common metals. In order to reduce the background to that seen in ^{3}He detectors, two methods are currently investigated – nickel plating of the aluminium to stop the emitted α's, and the use of specially purified aluminium. Respective costs will likely be the deciding factor between these two approaches.

A second significant difference with ^{3}He detectors is that the detector can be optimized for a specific wavelength or distribution of wavelengths [13]. The current prototype has 30 $^{10}B_4C$ layers of $1\,\mu m$, which is the optimal for $2.5\,\mathring{A}$ neutrons. This may or may not be the best configuration for a given instrument. For example, efficiency can be significantly increased using thinner layers, if only cold neutrons are of interest, however, in this case the efficiency for thermal neutrons will decrease. In case of ^{3}He by contrast, the only parameter is the total amount of the gas per detector area, and the trade-off in the example above does not occur.

As the following step in this project, a larger demonstrator is currently being built. This detector will have the dimensions and specifications of a module of IN5 [2]. With 15 times the sensitive area ($80 \times 300\,cm^2$), this detector will demonstrate the feasibility and cost of large-scale production of both the mechanical parts as well as the $^{10}B_4C$ layers required.

Acknowledgments
The work has been supported by the CRISP project (European Commission 7th Framework Programme Grant Agreement 283745).

References

[1] S. Peggs, *ESS Technical Design Report* (2013) http://europeanspallationsource.se/scientific-technological-documentation
[2] H. Mutka, J. Ollivier and L. Didier., *The new cold neutron time-of-flight spectrometer IN5*, *Neutron News* 21(2) (2010).
[3] R.T. Kouzes, *The 3He supply problem. Technical Report 18388*, *PNNL* (2009) page.
[4] GAO, *Neutron detectors: an alternative to using Helium-3. Technical Report 11-753*, *US Government Accountability Office* (2011).
[5] D. A. Shea and D. Morgan, *The Helium-3 shortage: Supply, demand, and options for congress. Technical Report R41419*, *Congressional Research Service* (2010).
[6] K. Zeitelhack, *Search for alternative techniques to helium-3 based detectors for neutron scattering applications*, Neutron News, 23:4 (2012), 10-13.
[7] A. Khaplanov *et al.*, *Multi-Grid Boron-10 detector for large area applications in neutron scattering science*, *arXiv:1209.0566* (2012).
[8] J. Correa *et al.*, *10B4C Multi-Grid as an Alternative to 3He for Large Area Neutron Detectors*, *Trans. Nucl. Sc.* (2013) DOI: 10.1109/TNS.2012.2227798.
[9] B. Guerard *et al.*, *10B multi-grid proportional gas counters for large area thermal neutron detectors*, *Nucl. Instr. Meth. A* (2012) http://dx.doi.org/10.1016/j.nima.2012.12.021.
[10] Patent no. 20110215251
[11] Y. Blanc, *Le Spectrometre A Temps De Vol IN6, characteristiques, techniques et performances*, report 83Bl21G (1983) http://www.ill.eu/nc/instruments-support/instruments-groups/instruments/in6/more/infofilestodownload/
[12] C. Höglund, *et al.*, *B_4C thin films for neutron detection*, *J. Appl. Phys.* 111(104908) (2012).
[13] F. Piscitelli and P. van Esch, *Analytical modeling of thin film neutron converters and its application to thermal neutron gas detectors*, JInst, 8, P04020, (2013).
[14] A. Khaplanov *et al.*, *Investigation of gamma-ray sensitivity of neutron detectors based on thin converter films* arXiv:1306.6247 (2013) *submitted to J. Inst.*
[15] D.P. Bouldin, *The measurement of alpha particle emissions from semiconductor memory materials* Journal of Electronic Materials, Vol. 10, No. 4 (1981).
[16] M. Leroy, *Alpha Rays Emitting Impurities in Ultra Pure Aluminum Evolution Through the Successive Refining Steps* Journal de Physique 111, Volume 5,(1995)
[17] J. Hofmann *et al.*, *"Nuclear Safety and the environment: Natural Radionuclide Concentrations in Materials Processed in the Chemical Industry and the Related Radiological Impact"*, DG-Environment Report EUR 19264 (2000)